Chemical Geology, 78 (1989) 229-244
Elsevier Science Publishers B.V., Amsterdam — Printed in The Netherlands

Dissolution kinetics of experimentally shocked silicate minerals*

RANDALL T. CYGAN[1], WILLIAM H. CASEY[1], MARK B. BOSLOUGH[2], HENRY R. WESTRICH[1], MARTIN J. CARR[3] and GEORGE R. HOLDREN, Jr.[4]

[1]*Geochemistry Division, Sandia National Laboratories, Albuquerque, NM 87185 (U.S.A.)*
[2]*Shock Wave and Structural Physics Division, Sandia National Laboratories, Albuquerque, NM 87185 (U.S.A.)*
[3]*Electron Optics and X-Ray Analysis Division, Sandia National Laboratories, Albuquerque, NM 87185 (U.S.A.)*
[4]*Northrop Services, Inc., Corvallis, OR 97333 (U.S.A.)*

(Accepted for publication August 18, 1989)

Abstract

Cygan, R.T., Casey, W.H., Boslough, M.B., Westrich, H.R., Carr, M.J. and Holdren, Jr., G.R., 1989. Dissolution kinetics of experimentally shocked silicate minerals. In: J. Schott and A.C. Lasaga (Editors), Kinetic Geochemistry. Chem. Geol., 78: 229-244.

The effect of lattice strain on mineral dissolution rates was examined by comparing the dissolution rates of shocked and unshocked minerals. Labradorite, oligoclase and hornblende were explosively shocked at mean pressures ranging from 4 to 22 GPa. The labradorite was examined with transmission electron microscopy to estimate the density of dislocations produced by the shock-loading experiment. Subsamples of the labradorite were then thermally annealed to remove some of the dislocations, and to evaluate the importance of such thermal pre-treatment in preparing mineral surfaces for experiments. The dissolution rates of these minerals were measured in batch experiments at pH-values of 2.7 and 4.0.

Shock-loading did not produce extremely high dislocation densities in the labradorite. The density of dislocations in the unshocked labradorite is $\leqslant 10^{10}\,m^{-2}$. After shocking, the density increases to $\sim 10^{12}$-$10^{13}\,m^{-2}$. The distribution of dislocations is heterogeneous, and the amount of deformation does not increase substantially with shock pressure. These results are highly atypical of shock-modified minerals, where relatively low shock pressures usually induce high ($\sim 10^{15}\,m^{-2}$) densities of dislocations. Thermal annealing for 1 hr. at 900°C in a dry furnace removes many dislocations from the shocked labradorite.

The difference in observed dissolution rates between shocked and unshocked minerals appears to have a weak correlation with the increase in the density of dislocations on the mineral surface. The unshocked and shocked oligoclase and hornblende samples exhibit limited dissolution enhancement at pH 4.0. Increasing the density of dislocations by several orders of magnitude with shock-loading causes a relatively small increase in dissolution rates for these silicate minerals. These results suggest that the surface dislocations produced by the shock treatment are not the primary sites for dissolution reactions.

1. Introduction

Interest in characterizing rates of natural weathering reactions has led to efforts to quantify rates of mineral dissolution. Researchers have emphasized the need to understand the role of crystal defects in controlling the reaction of rock-forming minerals with natural solutions. Many workers, for example, have noted that soil minerals dissolve preferentially at dis-

*Paper presented at the International Congress of Geochemistry and Cosmochemistry, Paris, France, August 29-September 2, 1988.

crete sites on the exposed surface, rather than by the uniform retreat of the mineral–fluid interface (e.g., Berner and Holdren, 1977, 1979; Brantley et al., 1986). Weathering at these discrete sites results in the formation of crystallographically controlled pits on the mineral surface, which relate to the exposure of dislocations in the mineral lattice onto the mineral surface (Lasaga, 1984; Brantley et al., 1986; Lasaga and Blum, 1986). Solution etching at these active sites may control the overall rate of dissolution of some minerals (e.g., Berner and Holdren, 1977) by providing a reactive site on the mineral with a low activation energy for dissolution.

If indeed the outcrop of lattice defects onto the mineral surface contributes to mineral dissolution, one expects to find a strong correlation between mineral hydrolysis rates and the abundance of dislocations (or the amount of strain) in the mineral. In general, however, researchers have found only a small relation between dissolution rates and dislocation densities or lattice strain. Murr and Hiskey (1981), for example, studied the relation between dissolution kinetics of strained chalcopyrite and the dislocation density. They found that the dissolution rate increased by approximately a factor of 2 as the dislocation density increased from 10^{11} to 10^{15} m^{-2}. A similar result is reported by Casey et al. (1988a) for strained rutile. Schott et al. (1989) report a small variation in the dissolution rate of calcite as the dislocation density varies from $\sim 10^{10}$ to $\sim 10^{14}$ m^{-2}. In some of these cases, the variation in mineral dissolution rate with dislocation density is entirely accounted for by the variation in the mineral activity with lattice strain. The contribution of the excavation of etch pits to the bulk dissolution rate may be much smaller than previously supposed. Thus, our understanding of the relation between lattice strain and mineral dissolution rates can be fruitfully extended by examining common rock-forming minerals, such as feldspar (see also Bosworth, 1981; Holdren et al., 1988; Murphy, 1988).

In this paper we examine the effect of experimental shock-loading on the dissolution rate of two feldspars and a hornblende. Although no concerted effort was made to simulate natural conditions of weathering, the dissolution experiments were designed for a relative comparison of dissolution rates as a function of shock pressure and dislocation density.

The primary hypothesis to be tested in this research is that dissolution rates of silicate minerals increase with lattice strain as induced by shock-loading. In only one of these minerals (calcic plagioclase) do we relate the shock and annealing conditions to dislocation densities. Therefore, in experiments with the other two minerals, we rely on the extensive previous research (e.g., Davison and Graham, 1979; Graham, 1981; Casey et al., 1988a) showing a strong relationship between shock-loading and dislocation densities. Shock-loading is a standard experimental technique for homogeneously deforming ceramic materials. Graham et al. (1986) provide a useful review of this technique and its application to materials science. Boslough and Cygan (1988) discuss the application of this technique to geological materials, and provide some data correlating dissolution rates with shock pressure. They also evaluate the role of shock-activated weathering in the formation of planetary surface material where impact-induced shocks are common (also see Boslough et al., 1986).

2. Experimental method

Two plagioclase minerals (labradorite and oligoclase) and a ferromagnesian mineral (hornblende) were selected for shock-loading. The oligoclase sample is from a nepheline syenite near Bancroft, Ontario, Canada, and the hornblende is from Mineral County, Nevada, U.S.A. The labradorite sample was collected from a weathered basalt flow near Pueblo Park, New Mexico, U.S.A., and has previously been identified as a bytownite plagioclase (see Boslough and Cygan, 1988; Casey et al., 1988b).

Both of the plagioclase samples are of high quality and show no evidence of twinning. The oligoclase and hornblende samples were ground and sieved to a size range of 37–149 μm in preparation for the shock-loading and unshocked dissolution experiments. The labradorite sample was split into two different size separates; one with an initial grain size range of 125–425 μm for the shock-loading and the other with a grain size range of 25–75 μm for the unshocked dissolution dissolution experiment. Chemical analyses provided by electron microprobe indicate the plagioclase feldspars to be of composition An_{25} for the oligoclase and An_{60} for the labradorite (Casey et al., 1988b). Microprobe scans across several single grains of both plagioclase indicated the samples to be chemically homogeneous. The hornblende sample has a composition along the hornblende–tremolite join and is best represented by a chemical formula of:

$$Ca_2(Mg_{3.3}Fe_{1.7})(Si_{7.5}Al_{0.5})O_{22}(OH)_2$$

Table I provides a summary of the mineral compositions based on the analysis of numerous mineral grains with an electron microprobe.

TABLE I

Chemical compositions of silicate minerals*[1]

Number of grains analyzed	Labradorite 48	Oligoclase 10	Hornblende 10
SiO_2	51.86 ± 0.57	62.15 ± 0.40	54.42 ± 1.06
TiO_2	0.07 ± 0.02	-	0.06 ± 0.03
ZrO_2	0.24 ± 0.02	-	-
Al_2O_3	29.62 ± 0.25	23.08 ± 0.36	1.29 ± 0.83
Fe_2O_3	0.69 ± 0.04*[2]	0.03 ± 0.03*[2]	-
FeO	-	-	13.78 ± 1.55*[2]
Mn_2O_3	0.01 ± 0.01*[2]	-	-
MnO	-	-	0.32 ± 0.19*[2]
MgO	0.10 ± 0.01	-	15.32 ± 0.99
BaO	0.03 ± 0.02	-	-
CaO	12.20 ± 0.12	5.06 ± 0.20	12.60 ± 0.27
Na_2O	4.22 ± 0.20	8.35 ± 0.12	0.20 ± 0.14
K_2O	0.30 ± 0.02	0.21 ± 0.10	0.09 ± 0.09
P_2O_5	0.20 ± 0.02	-	-
H_2O	< 0.001	-	1.91 ± 0.41*[3]
Total	99.54	98.88	99.99

*[1]Compositions reported in weight percent of oxide; uncertainty represents one standard deviation based upon multiple analyses.
*[2]Oxide values for multivalent ions determined by structural formula analysis based upon initial FeO and MnO analyses.
*[3]Obtained by difference.

Shock-recovery experiments on the three silicate minerals were performed using the Sandia National Laboratories "Bear" explosive loading fixtures. The fixtures were designed to provide well-characterized shock states such that the samples are shocked in a controlled and reproducible manner. The technique involves the generation of a plane wave that is directed and propagated through a powdered sample. The shock wave is produced by the detonation of a high explosive positioned above the fixture (see Graham and Webb, 1986; Casey et al., 1988a). The powdered sample is housed in a copper fixture beneath an iron pulse-forming plate. The conditions at the maximum shock state are determined using the numerical simulations of Graham and Webb (1984, 1986) based upon the geometry of the sample holder, the type of explosive, and the packing density of the mineral powder. A substantial portion of the sample can eventually be recovered from the copper fixture for post-shock examination or experiment.

Approximately 8 g of each mineral sample were shocked using the standard Sandia geometries and explosives (Table II). The minerals were shocked at three different mean peak pressures (7.5, 16 and 22 GPa). Approximately 2–3 g of shocked material were collected from slightly off-axis of the central core of the recovery fixture for each of the shock-loading experiments. This near-central region of the sample holder usually experiences the most uniform and homogeneous conditions of shock pressure and temperature (Graham and Webb, 1984). This hand-selected material was lightly disaggregated with a mortar and pestle then sonically washed in deionized water and acetone. Unshocked samples of each of the three minerals were treated similarly. Differences in

TABLE II

Shock experiments

Shot	Mineral	Fixture	Explosive	Sample compact density (mg m^{-3})	Sample compact density (%)	Mean peak pressure (GPa)	Estimated mean bulk temperature (°C)
*1*B*866*	oligoclase	Momma Bear	Baratol®	1.70	65	5-10	90-110
*2*B*866*		Momma Bear A	Baratol®	1.70	65	14-20	125-175
*3*B*866*		Momma Bear A	Comp B®	1.70	65	19-26	250-500
*1*B*876*	labradorite	Momma Bear	Baratol®	1.40	51	5-10	300-325
*2*B*876*		Momma Bear A	Baratol®	1.40	51	14-20	300-410
*3*B*876*		Momma Bear A	Comp B®	1.40	51	19-26	450-700
*4*B*876*		Papa Bear	Baratol®	1.68	62	3-5	80-100
*4*B*866*	hornblende	Momma Bear	Baratol®	2.30	77	5-10	25
*5*B*866*		Momma Bear A	Baratol®	2.30	77	14-20	50-75
*6*B*866*		Momma Bear A	Comp B®	2.30	77	19-26	125-275

chemical behavior between these two groups therefore represent the effects of the shock experiment. None of these shocked and unshocked mineral samples were heat-treated or annealed prior to the dissolution runs; the defect state of each of the minerals directly reflects the nature of the shock experiment or, for the unshocked samples, the conditions of mineral genesis and subsequent grinding history.

An additional shock experiment was conducted on the labradorite at a low peak pressure (4 GPa) to induce a relatively low concentration of dislocations. Subsamples of this material were subsequently thermally annealed, eliminating some strain from the mineral. By shocking the sample at a very low pressure (4 GPa), followed by varying temperatures of thermal annealing, we ultimately obtained samples of labradorite which had been deformed under a wide range of conditions (4, 7.5, 16 and 22 GPa, plus the annealed samples). These materials were subsequently examined by transmission electron microscopy (TEM) to characterize the effect of shock pressure and annealing on the microstructure of the mineral.

The importance of thermal annealing to dissolution experiments has been suggested as a means of producing uniform mineral surfaces (Barnes et al., 1983). To evaluate this possibility we examined the effect of annealing on mineral dissolution rates by heating the 4-GPa labradorite sample for 1 hr. at various temperatures. Subsamples of the shocked labradorite were annealed at 520°, 700° and 920°C in a dry furnace open to ambient pressure. The dissolution rates of these annealed samples were measured and compared with unshocked material, and the material which had been shocked but left unannealed.

Prior to the dissolution experiments, detailed characterization of separates from each of the shocked and unshocked samples was performed using several analytical techniques. All samples were examined with optical and scanning electron microscopy (SEM), and by powder X-ray diffraction (XRD). The labradorite samples were further examined by TEM.

Specific surface areas were determined by the multipoint adsorption isotherm of nitrogen gas and the BET method (Brunauer et al., 1938). We estimate the relative uncertainty for the surface area measurements to be $\sim \pm 6.5\%$, which corresponds to the overall coefficient of variation in a series of determinations obtained by Ace and Parsons (1979). The BET method is considerably more accurate in the measure-

ment of large surface areas (>2.0 m^2 g^{-1}), so we provide an estimate of $\pm 3.0\%$ for the relative uncertainty for these values. These uncertainties include both instrument and powder sampling variation, and differences in degassing behavior among samples and standards; it is a conservative estimate.

TEM was utilized to examine the texture and microstructure of the unshocked and shocked labradorite samples as well as the subsamples of the annealed material. Sample foils were prepared for TEM examination using the technique of Carr (1985), which was designed to avoid introducing spurious effects during sample manipulation. This technique involves placing ~ 100 mg of sample and a special epoxy mixture in a plastic tube. The assemblage is then centrifuged in order to concentrate the grains in a thin layer near the surface of the epoxy. After hardening of the epoxy and polishing of the mount surface, an ultrasonic cutter is used to slice thin disks from the mounted powder. The sample disks are dimpled and then ion milled with a 6-keV Ar^+ beam at a low grazing angle. The labradorite sample disks were examined with a JEOL® *200* CX electron microscope operating with a 200-keV beam. A JEOL® JSM T-*300* scanning electron microscope was utilized to obtain photomicrographs of the unshocked and shocked mineral surfaces in both pre- and post-dissolution condition.

The dissolution experiments were first performed on samples in each of the four states (unshocked, 7.5, 16 and 22 GPa) for each of the three minerals, providing twelve separate experimental runs, all under identical conditions. Each of the samples was reacted in a batch dissolution cell with a pH-buffered standard solution of 0.01 *N* potassium hydrogen phthalate. The standard solution provides an acidic environment with a nominal pH of 4 (measured pH = 4.05) which is maintained throughout the dissolution process. Although dissolved phthalate catalyzes aluminosilicate dissolution (Schindler and Stumm, 1987), the phthalate is assumed to affect each of the dissolution runs equally. Thus, the experiments are designed to provide *relative* dissolution rates. Approximately 1 g of each mineral sample was reacted with 200 ml of the standard solution. The dissolution cells were placed in a constant-temperature bath maintained at 25 °C and were kept agitated at a frequency of 1 c.p.s., except during the brief period of solution sampling. Continuous agitation of the cells tends to suspend the reacting mineral and disrupts any chemical diffusion layer which may form during mineral reaction, and thereby promotes a surface-controlled dissolution reaction. The dissolution cells were maintained at these conditions for up to 21 days. The cells were periodically sampled by removing a small volume of solution. An equal volume of unreacted solution was added to preserve a constant volume of solution in the reaction cell. The analytical data are corrected for this sampling procedure. Several additional labradorite dissolution experiments utilizing the thermally annealed samples were conducted at pH 2.7, rather than at pH 4.0. These dissolution experiments were performed in 0.002 *N* HCl solutions, but were otherwise identical to the experiments described above.

Silicon analyses were conducted using the colorimetric heteropoly-blue technique. This analytical technique utilizes an amino acid reducing agent to enhance the adsorption character of the silica–molybdate–phosphate complex that is obtained with the usual silicomolybdate analysis (A.P.H.A., 1970). Multiple Si analyses of samples and standards provided a relative precision and accuracy of $\sim \pm 5\%$ for the analytical technique. The solutions were also analyzed for Ca, Na and Al with a direct-current (DC) plasma emission spectrophotometer (Spectrometrics®-III). An estimate of $\pm 5\%$ uncertainty was obtained for the combined precision and accuracy for these analyses. In the present paper we are concerned only with the dissolution data for Si release. Boslough and Cygan (1988) provide the chemical analyses for the other major elements and a discussion of their leaching behavior.

3. Results

3.1. SEM *photomicrographs*

Examination of the mineral surface morphologies by SEM provides a convenient qualitative measure of the degree of shock-loading that the minerals experience. Figs. 1–3 provide a sequence of SEM photomicrographs for each of the different states of the minerals. These photomicrographs depict the mineral powders prior to dissolution. All three minerals exhibit brittle disaggregation. This is most apparent for the case of labradorite in which significant comminution and reduction of grain size has occurred and is a function of shock pressure (Fig. 1). The oligoclase samples exhibit significant (but less obvious) grain disaggregation and which also appears to increase with shock pressure (Fig. 2). No significant change or enhanced degree of comminution with shock-loading is readily apparent from the SEM photomicrographs for the hornblende samples (Fig. 3). These different responses to shock-loading suggest that the double chain structure gives the hornblende an inherently different elastic/plastic response to shock than the dense framework structure of the plagioclase minerals.

3.2. *Specific surface areas*

One quantitative measure of shock-induced changes in powder morphology is the specific surface area. In general, for materials below the

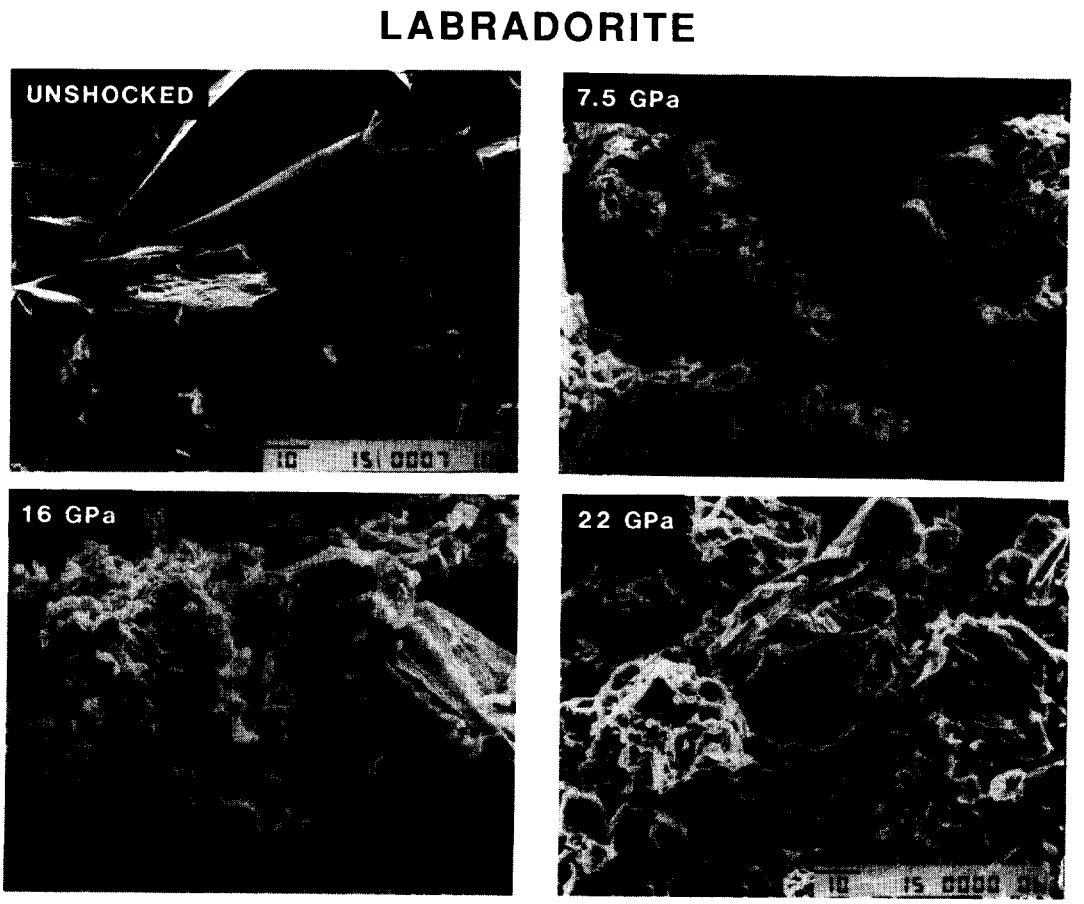

Fig. 1. Scanning electron photomicrographs of labradorite starting material and as recovered from three shock experiments. *Scale bar* in the lower right corner of each SEM photomicrograph denotes 10 μm.

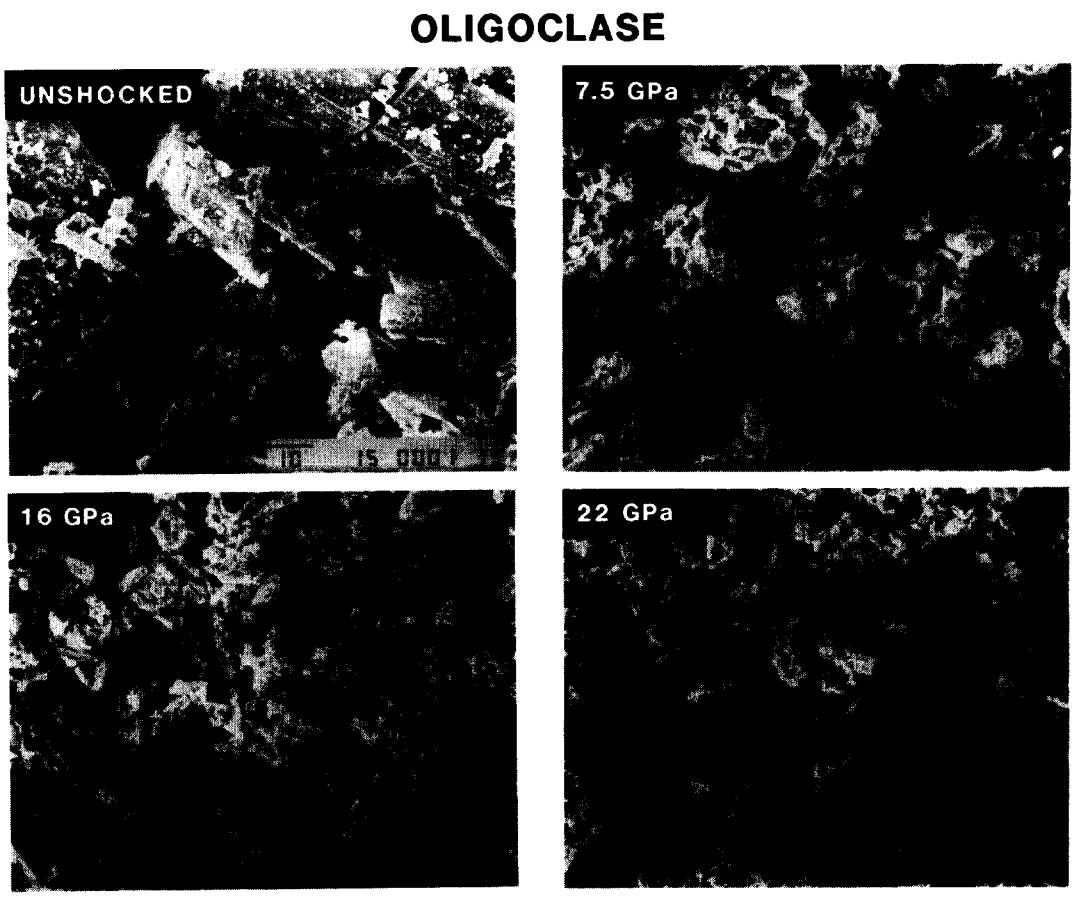

Fig. 2. Scanning electron photomicrographs of oligoclase starting material and as recovered from three shock experiments. For *scale bar*, see Fig. 1.

Hugoniot elastic limit one would expect shock deformation to create a relatively small change (~2-fold increase) in surface area; the shock energy is usually taken up by creating lattice defects and not by fracturing the material (see Wackerle, 1962). The specific surface areas for all of the mineral powder samples are compiled in Table III. Fig. 4 provides a graphical representation of the shocked mineral surface area relative to that of the unshocked phase as a function of shock pressure.

Note that the data for labradorite demonstrate a large variation in specific surface area and which may represent the response of the coarse-grained material to shock-loading. The labradorite samples shocked at 4 and 7.5 GPa exhibit roughly a 9-fold increase in specific surface area relative to the unshocked material, from 0.2 to 1.7 $m^2\ g^{-1}$. Such large increases in surface area suggest that pore space in the powder did not collapse entirely by plastic deformation during these shock experiments, and that much strain was taken up by crushing grains. Shock energy would be expected to first collapse all pore space in a porous plastic medium and then uniformly compress the contiguous grains. SEM and TEM photomicrographs of the labradorite powders indicate that some crystals in the powder were virtually undeformed while adjacent crystals were highly damaged. This type of inhomogeneous deformation is not typically observed in shock recovery experiments.

The variation in specific surface area be-

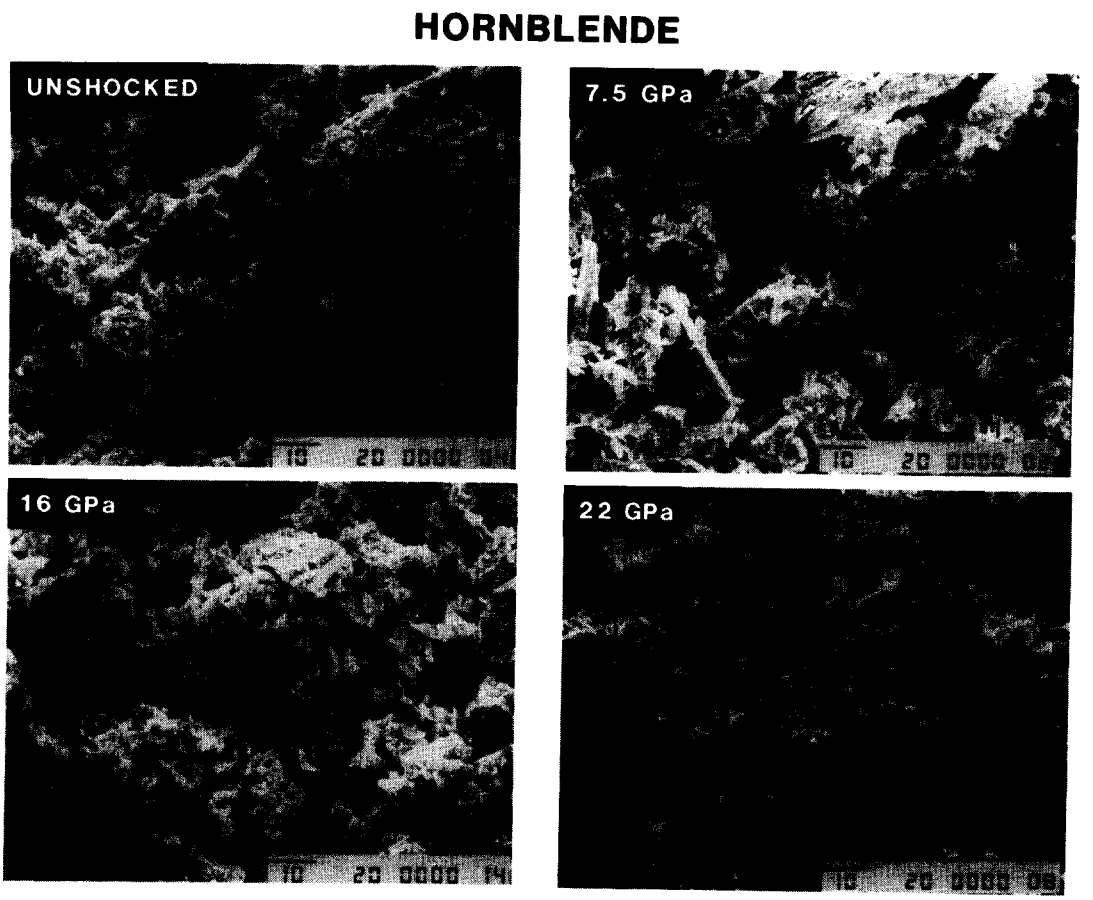

Fig. 3. Scanning electron photomicrographs of hornblende starting material and as recovered from three shock experiments. For *scale bar*, see Fig. 1.

tween shock pressures of 16 and 22 GPa for both labradorite and oligoclase is small relative to the total increase. Oligoclase and hornblende exhibit relatively small change in area over all shock pressures compared to labradorite (Table III). The smaller surface area increases at higher shock pressure may be due to more efficient plastic deformation of mineral grains during the shocking process at these higher pressures. The hornblende samples exhibit the smallest increases of surface area with shock pressure ($<40\%$). There was essentially no change in the specific surface area of the 22-GPa hornblende sample. These surface area data support the SEM observations of changes, or lack of change, in the microstructures of the minerals with increasing shock pressure.

3.3. Microstructure of shocked labradorite

Transmission electron photomicrographs of the labradorite before and after shocking at 4 GPa are shown in Fig. 5. The unshocked material is virtually dislocation-free and consists of coherent labradorite crystals with no evidence of deformation. Dislocation densities of this material are of the order of $\leqslant 10^{10}$ m^{-2}. Such low dislocation densities are near the limit of resolution of the TEM method. Only one dislocation could be identified in the material after examining many tens of grains.

Shock-loading created local areas of high deformation in this feldspar rather than the uniformly deformed material which is a typical product of shock experiments. Dislocations are

TABLE III

Specific surface areas, shock pressures, and rates of silicon release

Mineral	Mean peak shock pressure (GPa)	Anneal temperature (°C)	Specific surface area ($m^2 g^{-1}$)		Specific dissolution rate for Si (10^{-12} mol $m^{-2} s^{-1}$)	
			absolute	relative	absolute	relative
Oligoclase	unshocked		0.73 ± 0.05	1.00	0.45 ± 0.04	1.00
	7.5		3.01 ± 0.09	4.12 ± 0.13	4.9 ± 0.8	10.89 ± 1.78
	16.0		2.61 ± 0.08	3.58 ± 0.11	4.7 ± 1.3	10.44 ± 2.89
	22.0		2.38 ± 0.07	3.26 ± 0.10	6.0 ± 1.2	13.33 ± 2.67
Labradorite	unshocked		0.19 ± 0.01	1.00	6.7 ± 0.4	1.00
	unshocked		0.20 ± 0.01	1.00	93.0 ± 6.0*[1]	1.00
	4.0		1.71 ± 0.11	8.55 ± 0.56	72.0 ± 4.7*[1]	0.77 ± 0.05
	4.0*[2]	920	1.37 ± 0.09	6.85 ± 0.45	67.0 ± 4.4*[1]	0.72 ± 0.05
	4.0*[2]	700	1.57 ± 0.10	7.85 ± 0.51	84.0 ± 5.5*[1]	0.90 ± 0.06
	4.0*[2]	500	1.54 ± 0.10	7.70 ± 0.50	96.0 ± 6.2*[1]	1.03 ± 0.07
	7.5		1.72 ± 0.11	9.05 ± 0.59	13.2 ± 1.4	1.98 ± 0.21
	16.0		0.96 ± 0.06	5.05 ± 0.33	23.1 ± 2.4	3.46 ± 0.36
	22.0		1.14 ± 0.07	6.00 ± 0.39	17.0 ± 1.8	2.55 ± 0.27
Hornblende	unshocked		4.93 ± 0.15	1.00	1.2 ± 0.5	1.00
	7.5		6.72 ± 0.20	1.36 ± 0.04	2.6 ± 0.3	2.12 ± 0.26
	16.0		6.44 ± 0.19	1.31 ± 0.04	4.0 ± 0.4	3.31 ± 0.30
	22.0		4.86 ± 0.15	0.99 ± 0.03	4.5 ± 0.7	3.71 ± 0.58

*[1]Dissolution experiments performed at pH 2.7; all other results are for pH 4.0.
*[2]These samples were annealed at the listed temperature prior to dissolution; all other samples had no annealing treatment.

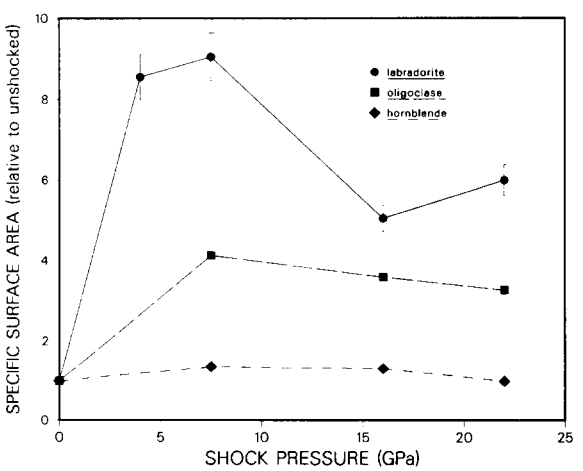

Fig. 4. Relative surface area for each of the three shocked minerals as a function of mean peak shock pressure. Surface areas are presented relative to the specific surface area of the unshocked phase. Error limits associated with the oligoclase and hornblende data are insignificant relative to the size of the data symbols.

concentrated in arrays associated with small cracks and in regions that are so highly deformed that individual dislocations cannot be resolved (see Fig. 5). These latter areas are observable in the photomicrographs as darkened regions. Locally, the density of dislocations increases to roughly 10^{12}–10^{13} m^{-2} with shock, as determined by comparing many TEM images, such as those of Fig. 5, with those from materials possessing well-characterized dislocation densities.

This estimate of dislocation density is uncertain because highly deformed regions represent $\leqslant 50\%$ of the area observed by TEM. Most grains are well crystallized and defect-free. Such well-annealed materials can be observed in Fig. 5 as expanses of uniformly shaded material, or material shaded only with broad fringes. This heterogeneous deformation contributes to the difficulty in interpreting the dissolution experiments. The total surface area of the mineral

Fig. 5. Transmission electron photomicrographs of labradorite: (a) before shock-loading; and (b) after 4-GPa shock. Note that damage to the mineral is not homogeneous, but is localized.

available for dissolution is expected to be proportional to, but not equal to, the area of highly reactive material. While this heterogeneity complicates the interpretation, the uncertainty is relatively small. That is, the average density of dislocations is certainly elevated well above that of the unshocked material. Thus, if excavation of dislocations (creating etch pits) during dissolution releases most of the mass of feldspar into solution, the dissolution rate of shocked material should be considerably higher than the unshocked material. Our primary hypothesis, that excavation of etch pits releases the most feldspar to solution, can still be tested.

We observe no significant difference in the TEM microstructure of labradorite shocked at different pressures – a highly unusual result for shock-modified materials. The microstructure of 4-GPa-shocked labradorite shown in Fig. 5, for example, is virtually identical to those observed for the feldspar shocked at 7.5, 16 and 22 GPa (not shown). The deformation is highly localized between areas of relatively undeformed material. Although dislocation densities are in the range of 10^{12}–10^{13} m^{-2} in local areas of high deformation, these represent $\leqslant 50$ areal percent of the material observed by TEM.

Annealing of the labradorite material at 920°C for 1 hr. removes most of the dislocations from the sample. Heating at lower temperatures does not dramatically change the microstructure of the material from the shocked state.

3.4. Evidence of phase changes

There was no evidence of new mineral formation for any of the shocked samples. However, significant line-broadening was observed in the XRD patterns for all of the shocked min-

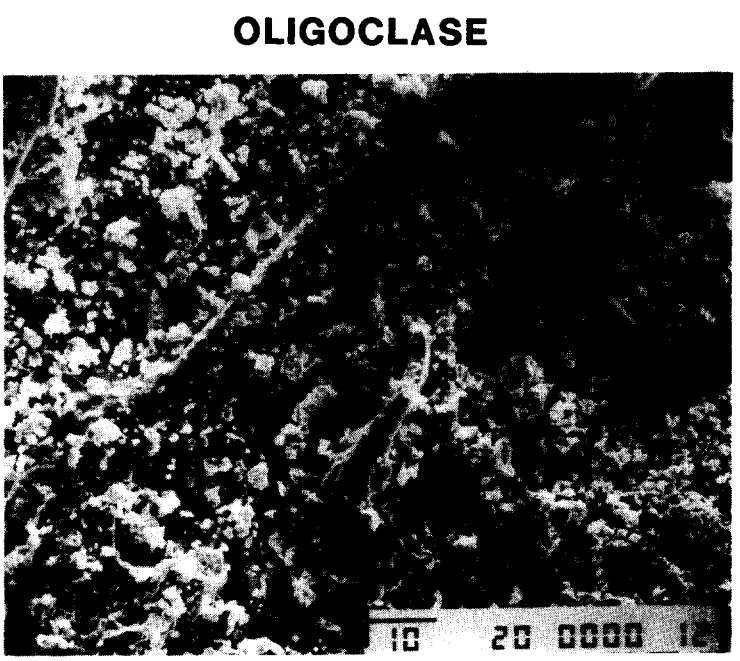

Fig. 6. Scanning electron photomicrograph of the outer layer of the sample cake for the oligoclase sample shocked to 22 GPa, exhibiting evidence of glass formation, localized melting and vesiculation.

erals. This is consistent with introduction of residual strain, a sizable variation in crystallite size, and possibly an increase in dislocation density, as a result of the shock-loading (see Morosin, 1986). There was no evidence of shock-generated glass in any of the shocked samples based upon the XRD patterns. However, SEM examination of the 22-GPa oligoclase sample indicated some morphological evidence of localized glass formation and melt texture (Fig. 6). Care was taken to avoid such material for use in the dissolution experiments. XRD and SEM analysis of the mineral powders upon completion of the dissolution experiments failed to detect the formation of any alteration phases.

3.5. Dissolution rates

In general, shock-loading does not dramatically induce an increase in the surface-area normalized dissolution rates of the three silicate minerals. The amount of Si released from a unit area of labradorite with time for shocked and unshocked samples at pH 2.7 is presented in Fig. 7. Si concentrations are normalized to account for the volume of solution in contact

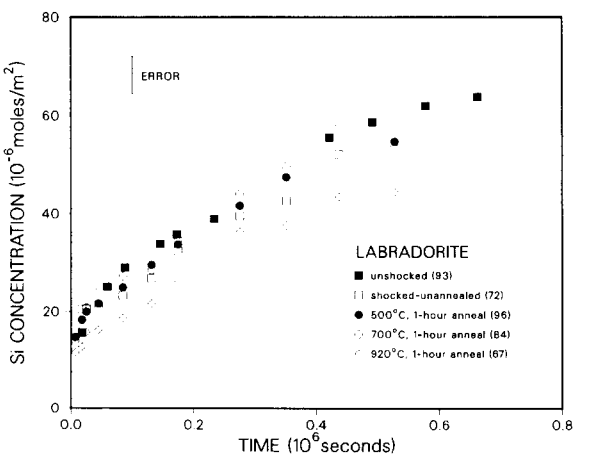

Fig. 7. Si concentration as a function of time for the dissolution of unshocked, shocked and shocked + annealed labradorite. Concentration is normalized to the volume of solution and the mineral surface area. Values for Si dissolution rate corresponding to steady-state slope of curves are provided parenthetically in units of 10^{-12} mol m^{-2} s^{-1}. All data were obtained from experimental runs performed at 25 °C and pH 2.7.

with the mineral, and for the total mineral surface area exposed to the solution. Expressed in this fashion, the slope of each curve in Fig. 7 corresponds to the Si release rate of that sample in units of mol m^{-2} s^{-1}. Data are included for unshocked labradorite, shocked labradorite, and labradorite which was annealed at various temperatures. All of the dissolution data presented in Fig. 7 are for the experiments conducted with the 0.002 *N* HCl solution (pH 2.7).

As can be seen in Fig. 7, after a short period of relatively rapid dissolution, Si concentration increases linearly with time for all samples. The initial nonlinear increase in concentration with time is probably created by the rapid dissolution of ultrafine particles adhering to the larger mineral grains. These ultrafine particles are produced during abrasion of the mineral powder and react rapidly with solution (Holdren and Berner, 1979). We attempted to remove the ultrafine material by pre-treating the starting material; however, the initial nonlinear behavior is observed in most of the dissolution curves.

The dissolution rate of unshocked labradorite, which has a dislocation density $< 10^{10}$ m^{-2}, is virtually identical to the shocked and unannealed material, which has an inhomogeneous dislocation density ranging from 10^{10} to 10^{13} m^{-2}. The observed variation in rate exhibited in Fig. 7 can almost entirely be accounted for by the uncertainty in the measurement of surface area. Similar results are reported by Murphy (1988) who examined the dissolution rates of strained sanidine. No difference in dissolution rates between strained and unstrained sanidine feldspar were observed over a similar range in dislocation densities as reported here for labradorite.

Hornblende and oligoclase exhibit a weak relationship between dissolution rate and shock pressure. Although no detailed TEM examinations were made of these shocked phases, we assume the dislocation densities are greatly increased by shock-loading in a fashion similar to that observed for labradorite. The dissolution experiments indicate measurable and possibly significant increases in the Si release rates between the unshocked and shocked samples of these minerals.

Data for hornblende dissolution at pH 4.0 are reported in Fig. 8, where we have compiled the Si-release history for both shocked and unshocked samples. These concentrations are also normalized to the specific area of each sample so that the slope of each curve is equivalent to the specific flux of Si from that mineral in units of mol m^{-2} s^{-1}. In a fashion similar to labradorite dissolution at pH 2.7, the hornblende exhibits Si concentration increasing approximately linearly with time after an initial period of rapid dissolution. The initial rapid and irregular period of dissolution is probably a result of the same process as mentioned earlier. We conclude that, although the shocked and unshocked hornblende samples differ in their early dissolution, after ~200 hr. the rates of Si release are within a factor of 4 for all samples. Thus, shock-loading has a relatively small effect upon the dissolution rate.

The Si and Al have different dissolution

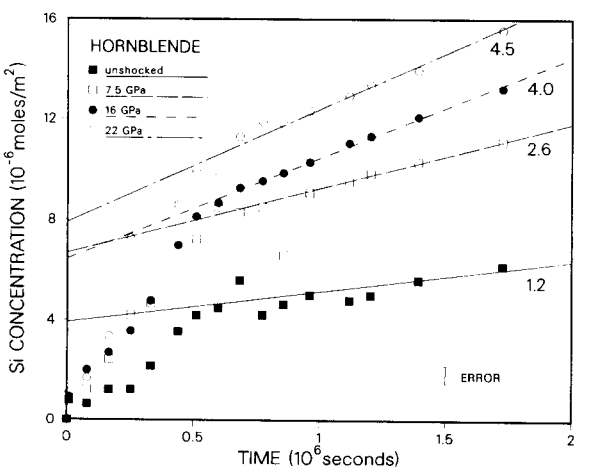

Fig. 8. Si concentration history for the dissolution of hornblende in each of four conditions: unshocked and recovered from three shock-loading experiments. Concentration is normalized to the volume of solution and the mineral surface area. Values for Si dissolution rates corresponding to steady-state slope of curves are provided in units of 10^{-12} mol m^{-2} s^{-1}. Data were obtained from experimental runs performed at 25 °C and pH 4.0.

fluxes from the hornblende surface after shocking (see figs. 6 and 7 of Boslough and Cygan, 1988). The hornblende results indicate an incongruent dissolution process with an ~4-fold (unshocked) and ~8-fold (16 GPa) difference in Si flux relative to Al throughout the dissolution process. A congruent dissolution, based upon the initial stoichiometry of the hornblende, would provide Si release rates which are 15 times that of Al. The shock-loading of the hornblende appears to shift the dissolution towards a more congruent leaching reaction.

Dissolution curves obtained at pH 4.0 for the unannealed labradorite and oligoclase samples appear to be weakly dependent on the effects of shock-loading (Figs. 9 and 10). For the case of labradorite, the shocked and unshocked materials differ in dislocation density by at least two orders of magnitude. However, the difference in reaction rate is less than a factor of 4. The oligoclase samples demonstrate a greater enhancement of dissolution with shock-loading than that exhibited by either labradorite or hornblende. It should be noted that some of the enhanced dissolution behavior of the shocked

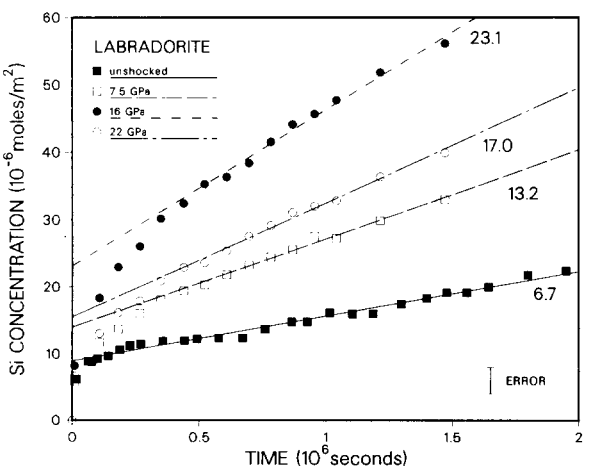

Fig. 9. Si concentration history for the dissolution of labradorite in each of four conditions: unshocked and recovered from three shock-loading experiments. Values for Si dissolution rates corresponding to steady-state slope of curves are provided in units of 10^{-12} mol m^{-2} s^{-1}. Data were obtained from experimental runs performed at 25 °C and pH 4.0.

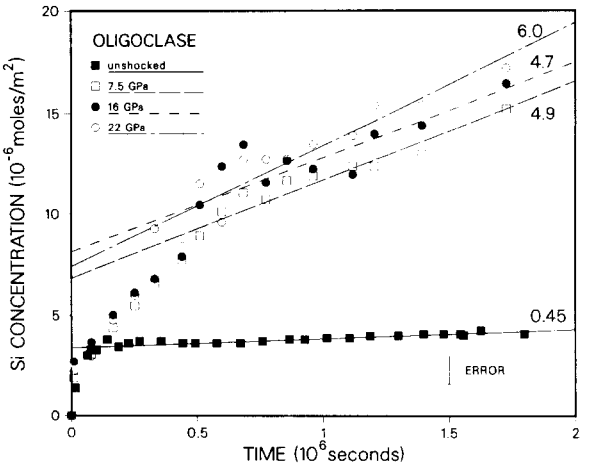

Fig. 10. Si concentration history for the dissolution of oligoclase in each of four conditions: unshocked and recovered from three shock-loading experiments. Values for Si dissolution rates corresponding to steady-state slope of curves are provided in units of 10^{-12} mol m^{-2} s^{-1}. Data were obtained from experimental runs performed at 25 °C and pH 4.0.

oligoclase can possibly be ascribed to the dissolution of glassy material generated during the shock (see Fig. 6), even though we were careful to avoid sampling the glassy fraction for the dissolution experiment. The dissolution of labradorite and oligoclase is incongruent with Al being leached in a molar amount similar to that of Si (non-stoichiometrically); shock pressure appears to have no effect upon this incongruency (see Boslough and Cygan, 1988).

Estimates of the mineral dissolution rates are compiled in Table III. A linear least-squares regression of each data set was used to determine the slope of the concentration per area vs. time curves and ultimately obtain the dissolution rate. The solution concentrations obtained after 166, 122 and 145 hr. of reaction were used from the hornblende, oligoclase and labradorite experiments, respectively, as the rates become linear beyond these times. The dissolution (Si release) rate, as denoted in these plots, is calculated from:

$$r = \frac{\Delta c}{\Delta t}\frac{V}{Am}$$

where $\Delta c/\Delta t$ is the rate of solution concentration change (mol l^{-1} s^{-1}); V is the solution volume (l); A is the initial specific surface area (m^2 g^{-1}); and m is the initial mass of the mineral (g). The resulting rate represents the specific dissolution rate in units of mol m^{-2} s^{-1} and corresponds to the slopes of the dissolution curves. In principle, the mineral mass and specific surface areas vary during the course of the reaction, but since the rates are extremely slow and the reaction times so short, these terms are treated as constants. Approximately 0.5–1% of each mineral is allowed to dissolve during the course of the experiment. The absolute dissolution rate is indicated for each of the concentration history curves presented in Figs. 7–10. The dissolution rates for the unshocked feldspars are consistent (within an order of magnitude) with those obtained for similar conditions by Holdren and Berner (1979) and Chou and Wollast (1984). Fig. 11 provides a graphical representation of the effect of the shock pressure upon the dissolution rate for each mineral relative to the rate obtained for the unshocked phase. Uncertainties for the absolute and relative dissolution rates presented in Table III and Fig. 11 represent the propagated errors associated with specific surface areas and the linear regressions.

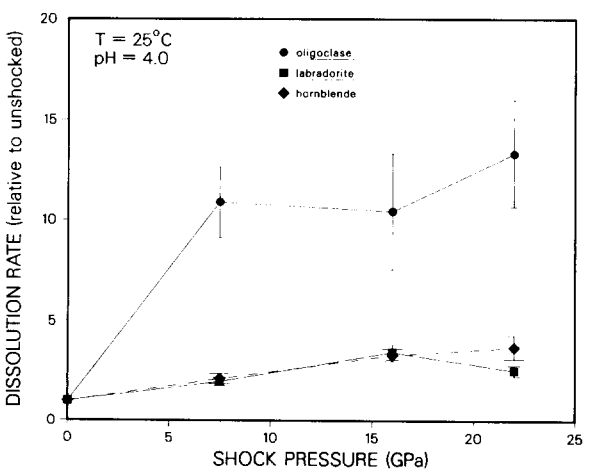

Fig. 11. Relative dissolution rate for each of the three shocked minerals as a function of mean peak shock pressure. Dissolution rates are presented relative to the absolute rate obtained for the unshocked phase. Only experimental data obtained at pH 4.0 are presented.

4. Discussion

The hypothesis that we tested in these experiments was that the excavation of the surface dislocations into etch pits contributed a large fraction of the dissolved mineral to solution. The excavation of etch pits, in other words, released much more mineral to solution than the uniform retreat of the mineral surface. For concentration of dislocations above a critical density, the rate of mineral dissolution should vary linearly with increases in the density of surface dislocation (Blum and Lasaga, 1987). However, we find that increasing the density of dislocations by several orders of magnitude with shock-loading causes a relatively small increase in dissolution rate for labradorite, oligoclase and hornblende.

There are two critical assumptions implicit in our dissolution experiments with these silicate minerals. For the case of oligoclase and hornblende, we first assume that shock-loading greatly increases the density of dislocations at the mineral surface relative to the unshocked sample. This assumption is probably justified given the results for labradorite (Fig. 5) and previous experience with shock-modification of ceramic materials (e.g., Casey et al., 1988a). A second assumption is that the dislocations produced by shock are energetically favored to form etch pits under the conditions of the dissolution experiment. There are inadequate data to test this second assumption for any of the minerals (see Brantley et al., 1986; Lasaga and Blum, 1986).

Reasons for the difference in the stoichiometry of hornblende dissolution with shock-loading are unclear. There are two viable explanations for this discrepancy. First, it is possible that the apparent difference in release rates is caused by the undetected precipitation of secondary phases during the dissolution experiment. At a pH of 4, the maximum concentra-

tions of Si and Al in the hornblende experiments ($\sim 180 \cdot 10^{-6}$ and $\sim 20 \cdot 10^{-6}$ *M*, respectively; Boslough and Cygan, 1988) were too low for extensive precipitation of simple secondary phases, such as gibbsite or halloysite (Holdren and Speyer, 1986). However, it is possible that aluminous phases precipitated and were not detected. The precipitation of smectite in one of the experiments, for example, would cause an apparent difference in the stoichiometry of hornblende dissolution with shock pressure.

A second, less likely, explanation is that shock-loading extensively changes the mechanism by which H^+ ions adsorb onto Al centers at the mineral surface. It is known that specific adsorption of hydrogen onto metal centers is related to the rate of dissolution (see Furrer and Stumm, 1986). In a mixed-oxide phase, such as hornblende, the coordination of hydrogen to Si or Al sites at the mineral surface are generally different, and this difference in coordination can cause incongruent dissolution in an acid solution (Chou and Wollast, 1984, 1985; Carroll-Webb and Walther, 1988). This second hypothesis cannot be tested without additional experiments.

5. Conclusions

The primary conclusion of this study is that shock-loading has a measurable but unexpectedly small effect on the aqueous dissolution rates of labradorite, oligoclase and hornblende. If we assume that shock greatly increases the dislocation densities in the minerals, we must conclude that excavation of etch pits at surface dislocations is not a major mechanism of mineral dissolution in these experiments. Increasing the density of dislocations by several orders of magnitude with shock-loading causes a relatively small increase in dissolution rates for these silicate minerals.

Acknowledgements

This research was performed at Sandia National Laboratories and was supported by the U.S. Department of Energy under contract DE-AC04-76DP00789. We wish to acknowledge the critical comments and thorough review provided by Susan Brantley. Michael Eatough and John Eichelberger provided constructive comments on an earlier draft of the paper. We also are appreciative of those who provided valuable advice and technical assistance during the course of this study, especially, M.U. Anderson, C.J. Daniel, K. Elsner, P.F. Hlava, J.L. Krumhansl, V.S. McConnell and C.T.C. Busters. The first author also acknowledges the Department of Geology of the University of Illinois for providing support during the final stages of this project.

References

Ace, H.L. and Parsons, D.S., 1979. Reproducibility of the surface area of some powders as measured by the Monosorb surface-area analyzer using the Brunauer-Emmett-Teller equation. J. Test Eval., 7: 334-337.

A.P.H.A. (American Public Health Association), 1970. Standard Methods for Examination of Water and Wastewater. Am. Publ. Health Assoc., New York, N.Y., 13th ed., 874 pp.

Barnes, H.L., Downs, W.F. and Rimstidt, J.D., 1983. Experimental determination of rates of hydrothermal reactions. In: Proceedings of the First International Symposium on Hydrothermal Reactions. Tokyo Inst. Technol., Tokyo, pp. 217-239.

Berner, R.A. and Holdren, G.R., 1977. Mechanisms of feldspar weathering: Some observational evidence. Geology, 5: 369-372.

Berner, R.A. and Holdren, G.R., 1979. Mechanism of feldspar weathering, 2. Observations of feldspars from soils. Geochim. Cosmochim. Acta, 43: 1173-1186.

Blum, A.E. and Lasaga, A.C., 1987. Monte Carlo simulations of surface reaction rate laws. In: W. Stumm (Editor), Aquatic Surface Chemistry. Wiley, New York, N.Y., pp. 255-292.

Boslough, M.B. and Cygan, R.T., 1988. Shock-enhanced dissolution of silicate minerals and chemical weathering on planetary surfaces. Proc. 18th Lunar Planet. Sci. Conf., pp. 443-453.

Boslough, M.B., Venturini, E.L., Morosin, B., Graham, R.A. and Williamson, D.L., 1986. Physical properties of shocked and thermally altered nontronite: Implications for the Martian surface. Proc. 17th Lunar Planet. Sci. Conf., J. Geophys. Res., 91: E207-E214.

Bosworth, W., 1981. Strain induced preferential dissolution of halite. Tectonophysics, 78: 509-525.

Brantley, S.L., Crane, S.R., Crerar, D.A., Hellmann, R. and Stallard, R., 1986. Dissolution at dislocation etch pits in quartz. Geochim. Cosmochim. Acta, 50: 2349-2378.

Brunauer, S., Emmett, P.H. and Teller, E., 1938. Adsorption of gases in multimolecular layers. J. Am. Chem. Soc., 60: 309-319.

Carr, M.J., 1985. A method of preparing powdered specimens for transmission electron microscopy. J. Electron Microsc. Tech., 2: 439-443.

Carroll-Webb, S.A. and Walther, J.V., 1988. A surface complex reaction model for the pH-dependence of corundum and kaolinite dissolution rates. Geochim. Cosmochim. Acta, 52: 2609-2623.

Casey, W.H., Carr, M.J. and Graham, R.A., 1988a. Crystal defects and the dissolution kinetics of rutile. Geochim. Cosmochim. Acta, 52: 1545-1556.

Casey, W.H., Westrich, H.R. and Arnold, G.W., 1988b. Surface chemistry of labradorite feldspar reacted with aqueous solutions at pH = 2, 3 and 12. Geochim. Cosmochim. Acta, 52: 2795-2807.

Chou, L. and Wollast, R., 1984. Study of the weathering of albite at room temperature and pressure with a fluidized bed reactor. Geochim. Cosmochim. Acta, 48: 2205-2217.

Chou, L. and Wollast, R., 1985. Kinetic study of the dissolution of albite with a continuous flow-through fluidized bed reactor. In: J.I. Drever (Editor), The Chemistry of Weathering. Reidel, New York, N.Y., pp. 75-96.

Davison, L. and Graham, R.A., 1979. Shock compression of solids. Phys. Rep., 55: 255-379.

Furrer, G. and Stumm, W., 1986. The coordination chemistry of weathering, I. Dissolution kinetics of δ-Al_2O_3 and BeO. Geochim. Cosmochim. Acta, 50: 1847-1860.

Graham, R.A., 1981. Active measurements of defect processes in shock-compressed metals and other solids. In: M.A. Meyers and L.E. Murr (Editors), Shock Waves and High-Strain Rate Phenomena in Metals - Concepts and Application. Plenum, New York, N.Y., pp. 375-386.

Graham, R.A. and Webb, D.M., 1984. Fixtures for controlled explosive loading and preservation of powder samples. In: J.R. Asay, R.A. Graham and G.K. Straub (Editors), Shock Waves in Condensed Matter, 1983. North Holland Publishing Co., New York, N.Y., pp. 211-214.

Graham, R.A. and Webb, D.M., 1986. Shock-induced temperature distributions in powder compact recovery fixtures. In: Y.M. Gupta (Editor), Shock Waves in Condensed Matter, 1985. Plenum, New York, N.Y., pp. 831-836.

Graham, R.A., Morosin, B., Venturini, E.L. and Carr, M.J., 1986. Materials modification and synthesis under high pressure shock compression. Annu. Rev. Mater. Sci., 16: 315-341.

Holdren, G.R. and Berner, R.A., 1979. Mechanism of feldspar weathering, 1. Experimental studies. Geochim. Cosmochim. Acta, 43: 1161-1171.

Holdren, G.R. and Speyer, P.M., 1986. Stoichiometry of alkali feldspar dissolution at room temperature and various pH values. In: S.M. Colman and D.P. Dethier (Editors), Rates of Chemical Weathering of Rocks and Minerals. Academic Press, New York, N.Y., pp. 61-81.

Holdren, G.R., Casey, W.H., Westrich, H.R., Carr, M. and Boslough, M., 1988. Bulk dislocation densities and dissolution rates in a calcic plagioclase. Int. Congr. of Geochemistry and Cosmochemistry, Eur. Assoc. Geochem., Chem. Geol., 70: 79 (abstract; special issue).

Lasaga, A.C., 1984. Chemical kinetics of water-rock interactions. J. Geophys. Res., 89: 4009-4025.

Lasaga, A.C. and Blum, A.E., 1986. Surface chemistry, etch pits and mineral-water reactions. Geochim. Cosmochim. Acta, 50: 2363-2379.

Morosin, B., 1986. X-ray diffraction line-broadening of shock-modified ceramic powders. In: R.A. Graham and A.B. Sawaoka (Editors), High Pressure Explosive Processing of Ceramics, Ch. 12. Trans Tech Publications, Aedermannsdorf, pp. 283-339.

Murphy, W.M., 1988. Dislocations and feldspar dissolution: Theory and experimental data. Int. Congr. of Geochemistry and Cosmochemistry, Eur. Assoc. Geochem., Chem. Geol., 70: 163 (abstract; special issue).

Murr, L.E. and Hiskey, J.B., 1981. Kinetic effects of particle-size and crystal dislocation density on the dichromate leaching of chalcopyrite. Metall. Trans., 12B: 255-267.

Schindler, D.W. and Stumm, W., 1987. The surface chemistry of oxides, hydroxides and oxide minerals. In: W. Stumm (Editor), Aquatic Surface Chemistry - Chemical Processes at the Particle-Water Interface. Wiley-Interscience, New York, N.Y., pp. 83-107.

Schott, J., Brantley, S.L., Crerar, D., Guy, C., Borcsik, M. and Willaime, C., 1989. Dissolution kinetics of strained calcite. Geochim. Cosmochim. Acta, 53: 373-382.

Wackerle, J., 1962. Shock-wave compression of quartz. J. Appl. Phys., 33: 922-937.